Computer Assisted Mechanics and Engineering Sciences, 13: 109–124, 2006.

Damage detection in elements of structures by the elastic wave propagation method

Wiesław Ostachowicz[1,3], Marek Krawczuk[2,3], Arkadiusz Żak[1], Paweł Kudela[1]

[1] *Faculty of Navigation, Gdynia Maritime University, Poland*
[2] *Faculty of Electrical and Control Engineering, Gdańsk University of Technology, Poland*
[3] *Institute of Fluid Flow Machinery, Polish Academy of Sciences, Gdańsk, Poland*

(Received in the final form February 15, 2006)

This paper presents certain results of the analysis of elastic wave propagation in one-dimensional (1-D) and two-dimensional (2-D) elements of structures with damage. The problem of the elastic wave propagation has been solved by the use of the Spectral Element Method (SEM). In this approach elements of structures are modelled by a number of spectral finite elements with nodes defined at appropriate Gauss-Lobatto-Legendre points. As approximation polynomials high order orthogonal Lagrange polynomials are used. In order to calculate the elements characteristic stiffness and mass matrices the Gauss-Lobatto quadrature has been applied. In the current analysis damage in the form of crack has been considered. It has been assumed that the damage can be of an arbitrary length, depth, and location and can be simulated as a line spring of varying stiffness. Numerical calculations illustrating the phenomena of the elastic wave propagation in isotropic media have been carried out for the case of an aluminium rod and beam as well as a flat aluminium panel and plate.

1. Introduction

A problem of damage detection in elements of structures remains one of the most challenging tasks to all classical damage detection methods. Techniques for detection of small damage must be based on high frequency excitation signals, while the use of any conventional modal method for that purpose becomes computationally inefficient. In the case of conventional modal methods the accuracy of a solved problem depends strongly on spatial finite element discretisation. It is well known that the mesh of finite elements must be very dense to reach high vibration modes, because only then any effects of wave scattering on structural discontinuities can be observed and captured [21]. Such an approach often leads to a large system of equations even for simple 1-D structures and solution of such systems is very time consuming. On the other hand on-line Structural Health Monitoring (SHM) systems require short computational times.

Over last few decades a variety of different numerical algorithms and techniques have been developed and used for the problem of elastic wave propagation. The most commonly used are the Finite Difference Method (FDM) [9, 10, 19, 28] and the Finite Element Method (FEM) [18, 25, 29, 30]. However, it should also be mentioned that the Boundary Element Method (BEM) [1, 2, 12, 23], the FFT-based (frequency-domain) Spectral Element Method (SEM) [7, 11, 21, 22] and the time-domain Spectral Element Method [14–16, 20, 24], the Mass-Spring Lattice Models (MSLM) [3, 27] as well as the Local Interaction Simulation Approach (LISA) [4–6] have been used and reported in the literature.

At this point it is necessary to distinguish clearly two different approaches to the SEM known in the literature. The first one, as mentioned before, is based on the Fast Fourier Transformation (FFT) and therefore is called *FTT-based* SEM [7, 11, 21, 22], whereas the second approach is a time domain method and is called *time-domain* SEM or simply SEM [14–16, 20, 24].

It seems that the FFT-based SEM approach, as proposed by Doyle [7], is a very effective numerical tool for wave propagation modelling of this class. In this approach additional throw-off elements are required due to periodic nature of the FFT and because of that fact the FFT-based SEM is well suited for solving problems of infinite or semi-infinite rods, beams, and plates. In order to overcome the problem of the periodic nature of the FFT the Laplace transform can be applied instead, as shown by Igawa [11]. However, it should be mentioned here that the use of the FFT limits the applicability of the FFT-based SEM to structures of rather simple geometry.

Opposite to the FFT-based SEM is placed, proposed by Patera [20], the time-domain SEM. The method is versatile and so far has found applications in the field of fluid dynamics [20], heat transfer, acoustics, as well as for modelling of the propagation of seismic waves. The method has been successfully applied to 2-D and 3-D problems related to elastic isotropic media as well as fully anisotropic media [14].

In this paper an efficient and accurate method has been used for the analysis of elastic wave propagation in 1-D and 2-D elements of structures with damage. The problem of the elastic wave propagation has been solved by the use of the time-domain SEM. In this approach elements of structures are modelled by a number of spectral finite elements with nodes defined at appropriate Gauss-Lobatto-Legendre points. As approximation polynomials high order orthogonal Lagrange polynomials are used. In order to calculate the elements characteristic stiffness and mass matrices the Gauss-Lobatto quadrature has been applied. In the current analysis damage in the form of crack has been considered. It has been assumed that the damage can be of an arbitrary length, depth, and location and can be simulated as a line spring with varying stiffness. Numerical calculations illustrating the phenomena of the elastic wave propagation in isotropic media have been carried out for the case of an aluminium rod and beam as well as a flat aluminium panel and plate. Although only isotropic elements of structures have been investigated in this work, the current approach can be easily extended for the use in the case of anisotropic (composite) materials as well as elements of complex geometry.

2. Spectral element method

The formulation of the Spectral Elements (SE) and calculation of the characteristic stiffness and mass matrices is very analogous to the classical Finite Element (FE) formulation. The main feature of the SE formulation is the adoption of specific shape functions possessing certain and desired properties. In the SE formulation a set of local shape functions in a spectral element is chosen as a set of orthogonal Lagrange polynomials. However, prior to this the degree N of the Legendre polynomials [17] must be chosen and the local nodes $\xi_i \in [-1,1]$, $i \in 1,\ldots,(N+1)$ within the element, in the local ξ-direction, are defined as the roots of the following equation,

$$(1-\xi^2)\,P'_N(\xi) = 0, \tag{1}$$

where $P'_N(\xi)$ denotes the first derivative of an appropriate Legendre polynomial of degree N. The local nodes specified in this way represent Gauss-Lobatto-Legendre (GLL) points. For the case of $N = 5$ the nodal coordinates of an 6-node spectral element can be defined as,

$$\begin{aligned} &\xi_1 = -1, \qquad \xi_2 = -\sqrt{\tfrac{1}{3}+\tfrac{2}{3\sqrt{7}}}, \qquad \xi_3 = -\sqrt{\tfrac{1}{3}-\tfrac{2}{3\sqrt{7}}}, \\ &\xi_4 = \sqrt{\tfrac{1}{3}-\tfrac{2}{3\sqrt{7}}}, \qquad \xi_5 = \sqrt{\tfrac{1}{3}+\tfrac{2}{3\sqrt{7}}}, \qquad \xi_6 = 1\,. \end{aligned} \tag{2}$$

It can be seen that for a chosen set of the element nodes Lagrange approximation polynomials $\phi_i(\xi)$, $i \in 1,\ldots,(N+1)$ can be formulated. These polynomials are the N-th order polynomials passing through the $(N+1)$ GLL points, while the internal nodes of the element are located at the positions which correspond to zeros of the Legendre polynomials. It can be shown theoretically that

such a distribution of nodes within an element results in the highest interpolation accuracy [24]. Moreover, it can also be shown that the approximation polynomials are orthogonal, i.e.

$$\int_{-1}^{1}\int_{-1}^{1} \phi_n(\xi)\phi_m(\eta)\,\mathrm{d}\xi\mathrm{d}\eta = \beta\delta_{nm}\,, \qquad n,m = 1,\ldots,(N+1), \tag{3}$$

where β is a certain constant and δ_{nm} denotes the Kronecker delta.

The method of calculation of the characteristic stiffness and mass matrices of a spectral finite element, without loosing any generality, can be demonstrated on the example of a simple 1-D, 6-node spectral rod finite element, presented in Fig. 1. The longitudinal displacement u within the element, measured along the x-axis, can be approximated as

$$u(\xi) = \mathbf{\Phi}(\xi)\{u\} = \sum_{i=1}^{N+1} \phi_i(\xi)\, u_i\,, \tag{4}$$

where $\mathbf{\Phi}(\xi)$ is the shape function matrix and $\{u\}$ is the vector of nodal degrees of freedom of the element. The element shape functions $\phi_i(\xi)$ (i.e. Lagrange approximation polynomials) are presented in Fig. 2.

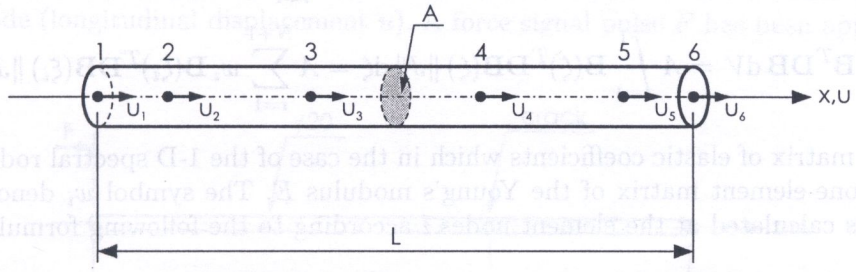

Fig. 1. 1-D, 6-node spectral rod finite element

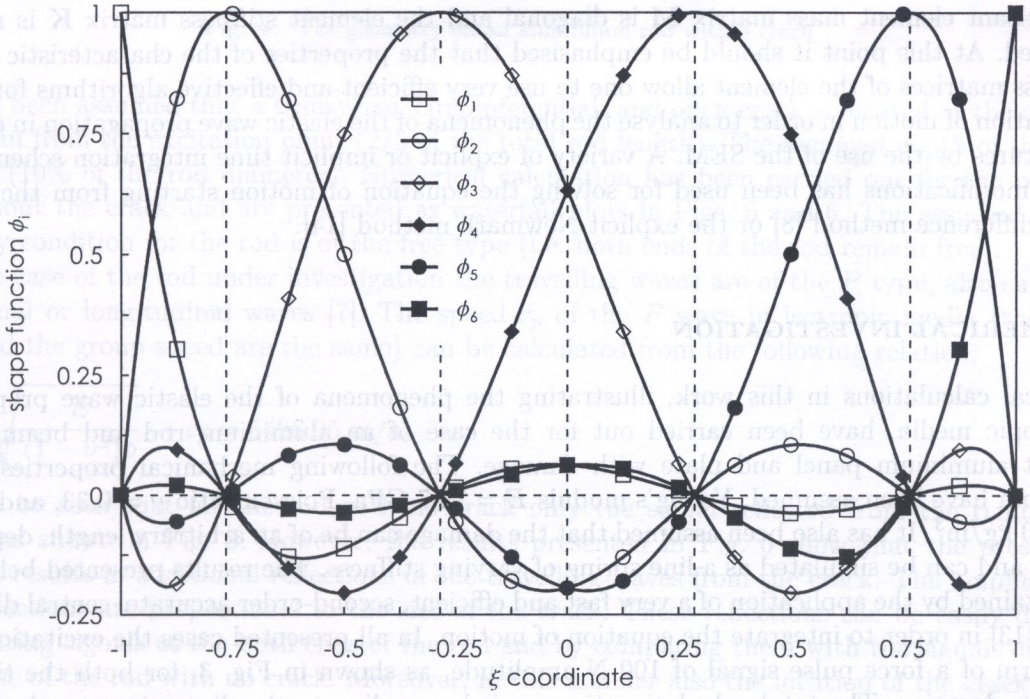

Fig. 2. Shape functions of a 1-D, 6-node spectral rod finite element

Based on the given displacement field the strains within the element can be expressed according to the well-known FE formula,

$$\epsilon_x(\xi) = \mathbf{B}(\xi)\{u\} = \sum_{i=1}^{N+1} B_i(\xi)\, u_i\,, \tag{5}$$

where $\mathbf{B}(\xi)$ represents the strain-displacement matrix, which can be calculated from

$$B_i(\xi) = \partial_x \phi(\xi) = J^{-1} \partial_\xi \phi(\xi) = \sum_{i=1}^{N+1} B_i(\xi), \tag{6}$$

and where J^{-1} denotes the inverse of the Jacobian matrix [13, 25, 29]. Following based on the shape function matrix $\mathbf{\Phi}(\xi)$ as well as the strain-displacement matrix $\mathbf{B}(\xi)$ the element stiffness and mass matrices can be easily calculated according to the well-known FE formula [13, 25, 29] as

$$\mathbf{M} = \rho \iiint_V \mathbf{\Phi}^T \mathbf{\Phi}\, \mathrm{d}V = \rho A \int_{-1}^{1} \mathbf{\Phi}(\xi)^T \mathbf{\Phi}(\xi)\, \|J\|\, \mathrm{d}\xi = \rho \sum_{i=1}^{N+1} w_i\, \mathbf{\Phi}(\xi_i)^T \mathbf{\Phi}(\xi_i)\, \|J_i\|, \tag{7}$$

$$\mathbf{K} = \iiint_V \mathbf{B}^T \mathbf{D} \mathbf{B}\, \mathrm{d}V = A \int_{-1}^{1} \mathbf{B}(\xi)^T \mathbf{D} \mathbf{B}(\xi)\, \|J\|\, \mathrm{d}\xi = A \sum_{i=1}^{N+1} w_i\, \mathbf{B}(\xi_i)^T \mathbf{D} \mathbf{B}(\xi_i)\, \|J_i\|, \tag{8}$$

where $\mathbf{D}$ is the matrix of elastic coefficients which in the case of the 1-D spectral rod finite element, simplifies to a one-element matrix of the Young's modulus E. The symbol w_i denotes the Gauss-Lobatto weights calculated at the element nodes i according to the following formula [17],

$$w_i = \frac{2}{N(N+1)[P_N(\xi_i)^2]}\,, \qquad i \in 1, \ldots, (N+1). \tag{9}$$

Because of the orthogonality of the approximation shape functions $\phi_i(\xi)$, as shown in Eq. (3), the resultant element mass matrix $\mathbf{M}$ is diagonal and the element stiffness matrix $\mathbf{K}$ is not fully populated. At this point it should be emphasised that the properties of the characteristic stiffness and mass matrices of the element allow one to use very efficient and effective algorithms for solving the equation of motion in order to analyse the phenomena of the elastic wave propagation in elements of structures by the use of the SEM. A variety of explicit or implicit time integration schemes with various modifications has been used for solving the equation of motion starting from the explicit central difference method [8] or the explicit Newmark method [14].

3. Numerical investigation

Numerical calculations in this work, illustrating the phenomena of the elastic wave propagation in isotropic media, have been carried out for the case of an aluminium rod and beam as well as a flat aluminium panel and plate with damage. The following mechanical properties for the aluminium have been assumed: Young's moduls $E = 72.7$ GPa, Poisson ratio $\nu = 0.33$, and density $\rho = 2700$ kg/m^3. It has also been assumed that the damage can be of an arbitrary length, depth, and location and can be simulated as a line spring of varying stiffness. The results presented below have been obtained by the application of a very fast and efficient, second-order accurate, central difference scheme [13] in order to integrate the equation of motion. In all presented cases the excitation signal has a form of a force pulse signal of 100 N amplitude, as shown in Fig. 3, for both the time and frequency domains. The total calculation time varied according to the dimensions on the element under consideration and in each case has been divided into 5000 time steps.

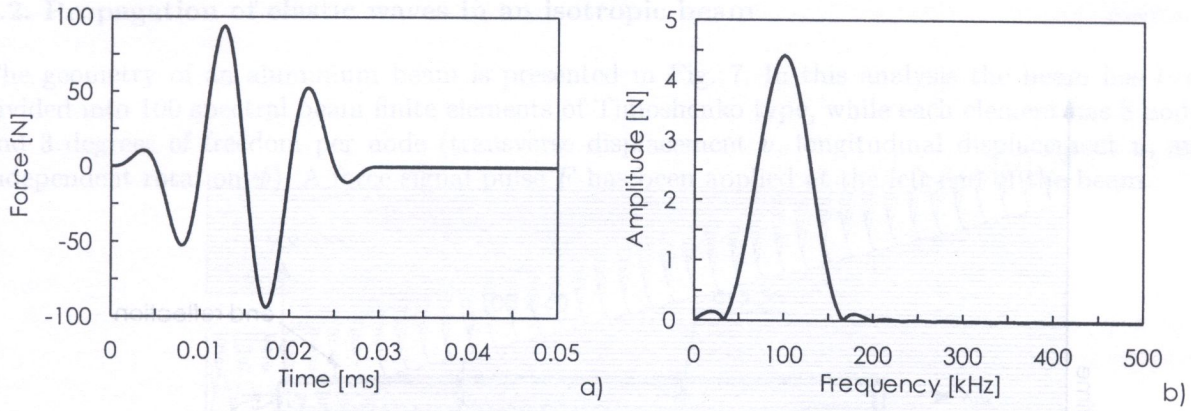

Fig. 3. An excitation signal in the form of a force pulse signal in: a) time, b) frequency domains

3.1. Propagation of elastic waves in an isotropic rod

The geometry of an aluminium rod is presented in Fig. 4. For the present analysis the rod has been divided into 100 spectral rod finite elements, while each element has 8 nodes and 1 degree of freedom per node (longitudinal displacement u). A force signal pulse F has been applied at the left end of the rod.

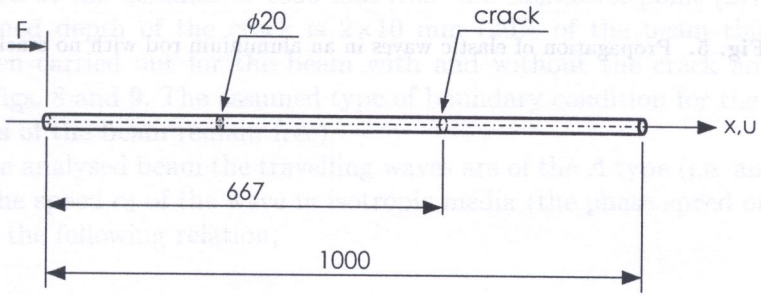

Fig. 4. The geometry on an aluminium rod with a crack

It has been assumed that a transverse, circumferential, and open crack is located at the distance of 667 mm from the excitation point (2/3 of the total rod length). The assumed depth of the crack is 2 mm (10% of the rod diameter). Numerical calculation has been carried out for the rod with and without the crack and are presented as waterfall plots in Figs. 5 and 6. The assumed type of boundary condition for the rod is of the free type (i.e. both ends of the rod remain free).

In the case of the rod under investigation the travelling waves are of the P type, also called the dilatational or longitudinal waves [7]. The speed c_p of the P wave in isotropic media (the phase speed and the group speed are the same) can be calculated from the following relation,

$$c_p = \sqrt{\frac{E}{(1-\nu^2)\rho}} \rightarrow c_p = 5496.95 \text{ m/s}. \tag{10}$$

It can be seen that for the rod with no crack only the signal reflected from the right end is present, as shown in Fig. 5. However, the results presented in Fig. 6 show that the presence of the crack results in additional reflections of the travelling waves from the crack. The amplitudes of these reflections are proportional to the size of the crack. These reflections can be easily detected by measuring signals at the both ends of the rod and by comparing them with the signals obtained in the case of the rod with no crack. Moreover, in this manner also the location of the crack can be evaluated, based on the known speed c_p of the propagation of the elastic P wave in aluminium and by measuring the time lags between the reflected signals at the rod ends.

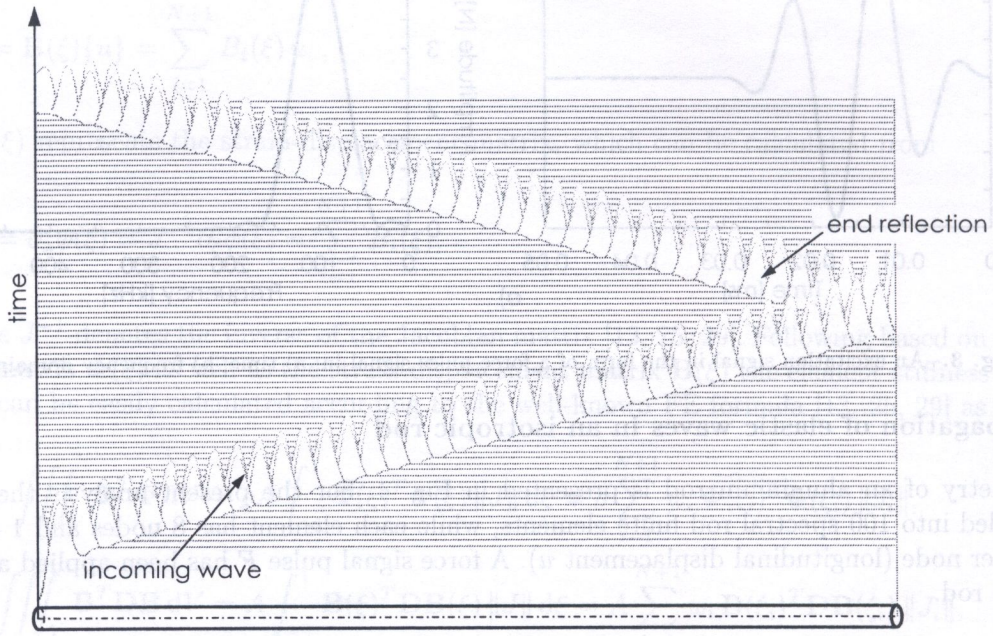

Fig. 5. Propagation of elastic waves in an aluminium rod with no crack

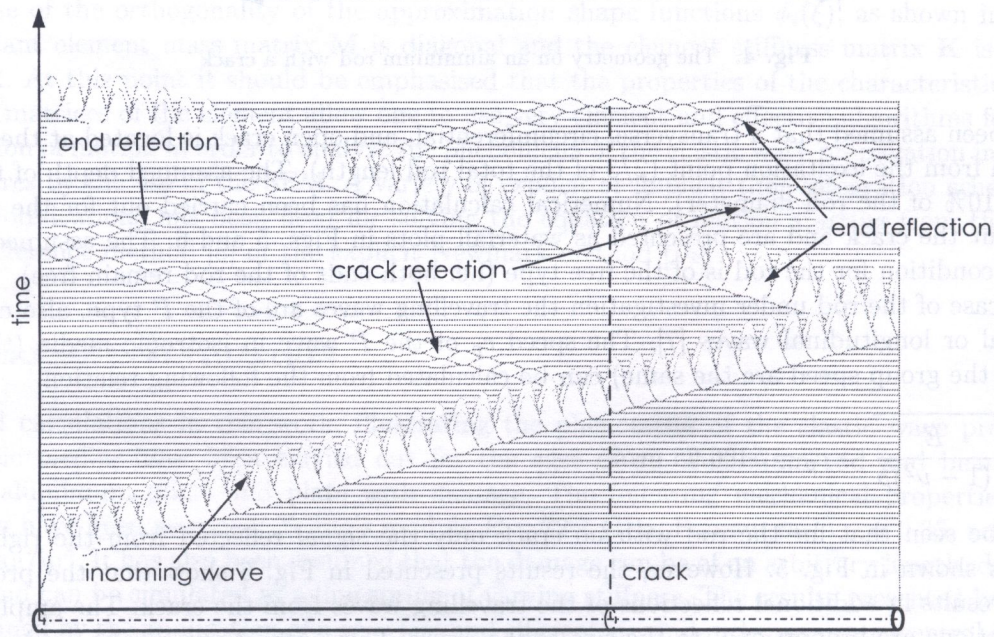

Fig. 6. Propagation of elastic waves in an aluminium rod with a crack

3.2. Propagation of elastic waves in an isotropic beam

The geometry of an aluminium beam is presented in Fig. 7. In this analysis the beam has been divided into 100 spectral beam finite elements of Timoshenko type, while each element has 8 nodes and 3 degrees of freedom per node (transverse displacement v, longitudinal displacement u, and independent rotation ψ). A force signal pulse F has been applied at the left end of the beam.

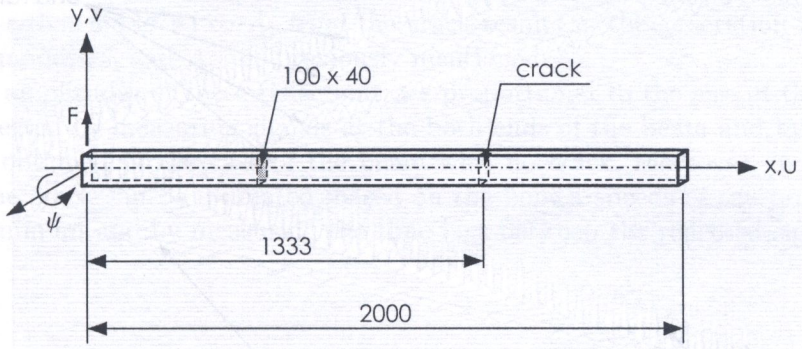

Fig. 7. The geometry on an aluminium beam with a crack

It has been assumed that a transverse, extending to the full width of the beam, and open double-edge crack is located at the distance of 1333 mm from the excitation point (2/3 of the total beam length). The assumed depth of the crack is 2×10 mm (20% of the beam thickness). Numerical calculation has been carried out for the beam with and without the crack and are presented as waterfall plots in Figs. 8 and 9. The assumed type of boundary condition for the beam is of the free type (i.e. both ends of the beam remain free).

In the case of the analysed beam the travelling waves are of the A type (i.e. anti-symmetric mode of Lamb waves). The speed c_0 of the wave in isotropic media (the phase speed of the A_0 mode) can be calculated from the following relation,

$$c_0 = \sqrt{\omega}\sqrt[4]{\frac{EI}{\rho A}} \rightarrow c_0 = 3067.97 \text{ m/s}. \tag{11}$$

where $\omega = 2\pi f$ and f is the average frequency of the excitation carrier wave, which in the case of the excitation signal presented in Fig. 3 is equal to 100 kHz. The combination coefficient EI denotes the flexural stiffness of the beam, A is the area of cross-section, and I is the second moment of area.

It should be noticed here that there are two modes A_0 and A_1 propagating in the beam at different propagation speeds, as shown in Fig. 8. It is well seen that the propagation speed of the A_0 mode is smaller that the propagation speed of the A_1 mode. The presence of the higher mode A_1 is due to the fact that the excitation signal has components of frequencies higher than so-called *cut-off* frequency f_c, for the given geometry and material of the beam. For excitation frequencies below the cut-off frequency f_c only the A_0 mode is propagating in the beam. On the other hand if the excitation frequency is higher than the cut-off frequency f_c the higher A_1 mode is also observed. Obviously the presence of even higher modes A_2, A_3, etc., requires excitations above the appropriate cut-off frequencies. The cut-off frequency f_c for the A_1 mode can be estimated from the following simple formula [7],

$$f_c = \frac{1}{2t}\sqrt{\frac{G}{\rho}} \rightarrow f_c = 22.5 \text{ kHz}, \tag{12}$$

where G is the shear moduls and t denotes the thickness of the beam.

It can be seen that for the case of the beam with no crack that the wave propagation pattern obtained and presented in Fig. 8 is similar to those obtained in the case of the undamaged rod.

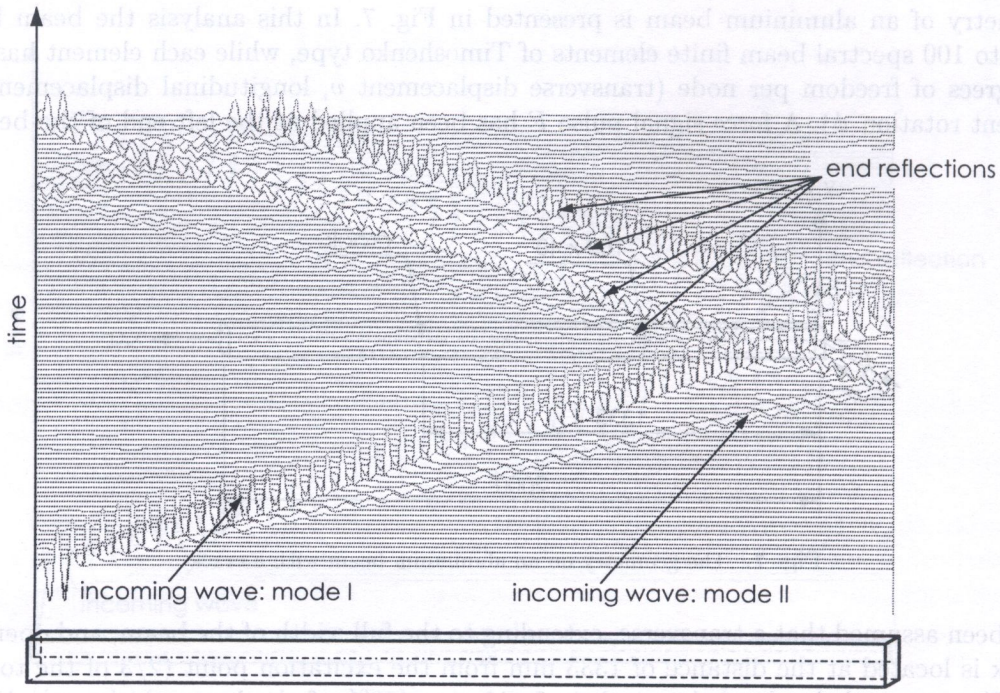

Fig. 8. Propagation of elastic waves in an aluminium beam with no crack

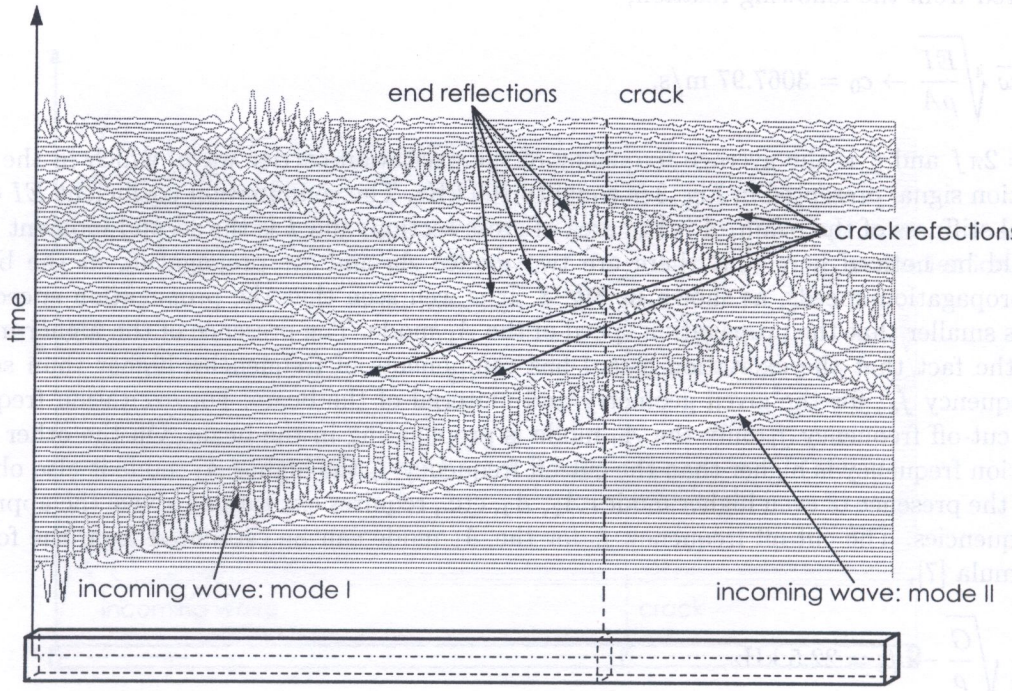

Fig. 9. Propagation of elastic waves in an aluminium beam with a crack

Because the waves are travelling in the beam as the modes A_0 and A_1 their reflections from the right end of the beam are clearly observed. It should be noted here that the reflections of either the mode A_0 or A_1 from the right end of the beam results in the generation of two new waves travelling as the modes A_0 and A_1 as well.

The presence of the crack in the beam results in the wave propagation patter being more complex. Besides the waves reflected from the right end of the beam, and travelling as the modes A_0 and A_1, additional reflections from the crack location are also clearly visible, as shown in Fig. 9. In this case the reflections of either mode A_0 or A_1 from the crack results in the generation of two new waves travelling as the modes A_0 and A_1 , as previously mentioned.

As before the amplitudes of these reflections are proportional to the size of the crack and they can be easily detected by measuring signals at the both ends of the beam and by comparing them with the signals obtained in the case of the beam with no crack. Moreover, in this manner also the location of the crack can be evaluated, based on the known speeds of the propagating A_0 and A_1 modes in aluminium and by measuring the time lags between the reflected signals at the beam ends.

3.3. Propagation of elastic waves in a flat isotropic panel

The geometry of a flat aluminium panel is presented in Fig. 10. For the present analysis the panel has been divided into 1600 spectral membrane finite elements with a regular mesh of 40×40 elements, while each element has 36 nodes and 2 degrees of freedom per node (longitudinal displacements u and v). A force signal pulse F has been applied at the centre of the panel and in the direction of the y-axis.

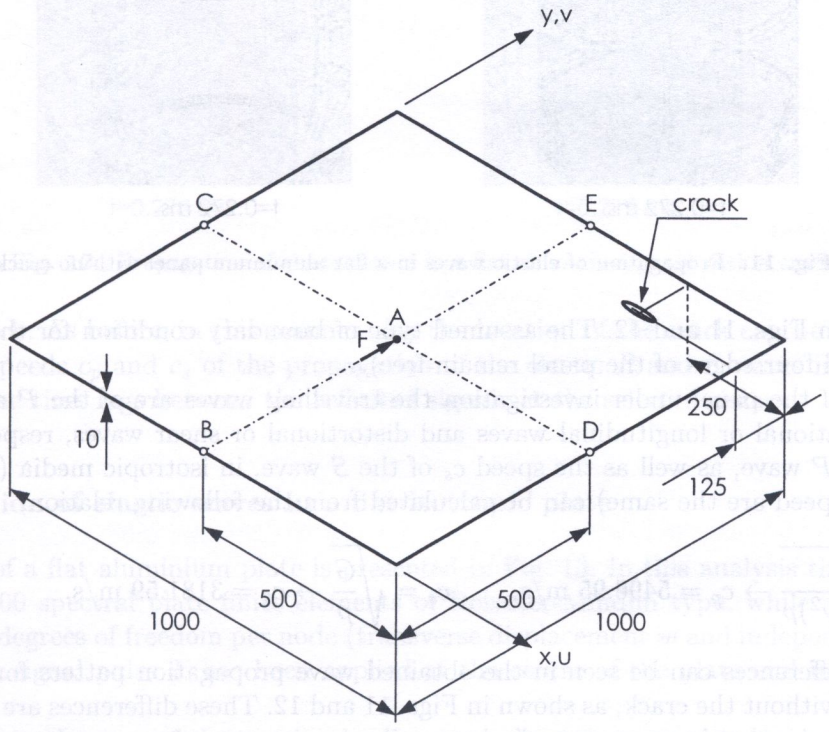

Fig. 10. The geometry on a flat aluminium panel with a crack

It has been assumed that a transverse and open crack is located at the distance of 125 mm from top edge of the panel and 250 mm from the right edge. The assumed depth of the crack is 2 mm, which is equivalent to 20% of the panel thickness. Numerical calculation has been carried out for the panel with and without the crack and are presented as maps of displacements u and v at 3 different

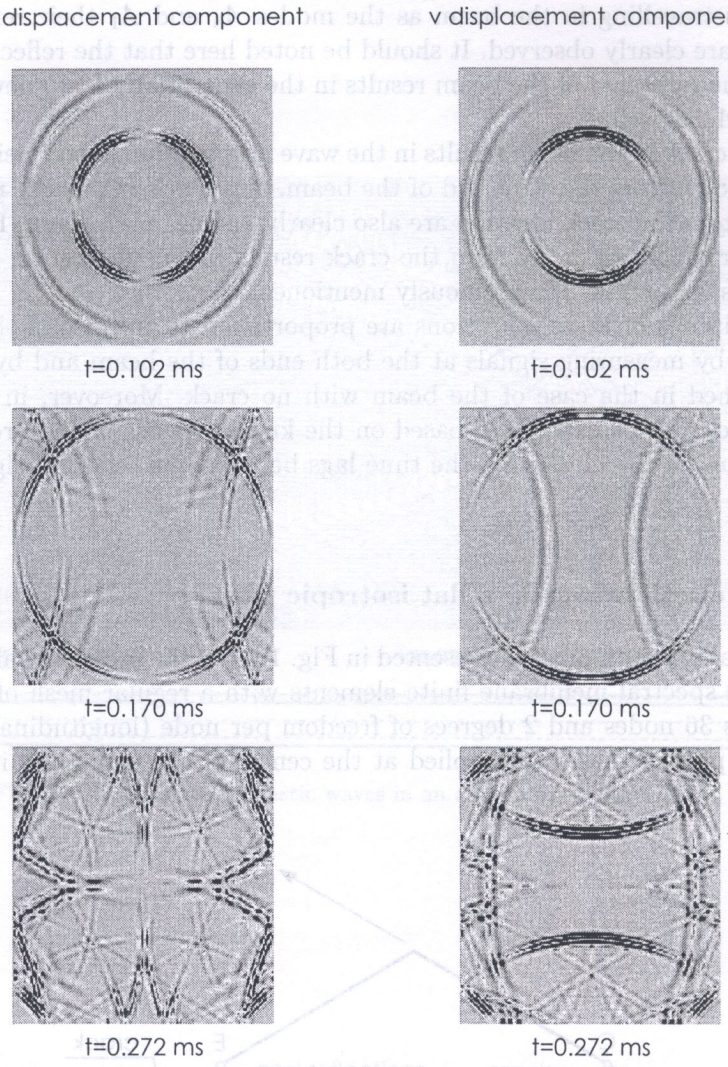

Fig. 11. Propagation of elastic waves in a flat aluminium panel with no crack

time instances in Figs. 11 and 12. The assumed type of boundary condition for the panel is of the free type (i.e. all four edges of the panel remain free).

In the case of the panel under investigation the travelling waves are of the P and S type, also called the dilatational or longitudinal waves and distortional or shear waves, respectively [7]. The speed c_p of the P wave, as well as the speed c_s of the S wave, in isotropic media (the phase speed and the group speed are the same) can be calculated from the following relation,

$$c_p = \sqrt{\frac{E}{(1-\nu^2)\rho}} \rightarrow c_p = 5496.95 \text{ m/s}, \qquad c_s = \sqrt{\frac{G}{\rho}} \rightarrow c_s = 3181.59 \text{ m/s}. \tag{13}$$

Significant differences can be seen in the obtained wave propagation patters for the case of the panel with and without the crack, as shown in Figs. 11 and 12. These differences are very well visible for both displacement components u and v.

Additional reflections of the travelling P and S waves from the crack can be seen (see Fig. 12) and the amplitudes of these reflections are proportional to the size of the crack. However, it should be said that the signal reflections from the crack generated by the P wave are, in general, weaker than the reflections generated by the S wave. The reflections can be easily detected by measuring signals at a number of points located on the panel surface (for example at points A, B, C, D, and E as shown in Fig. 10) and by comparing them with the signals obtained in the case of the panel

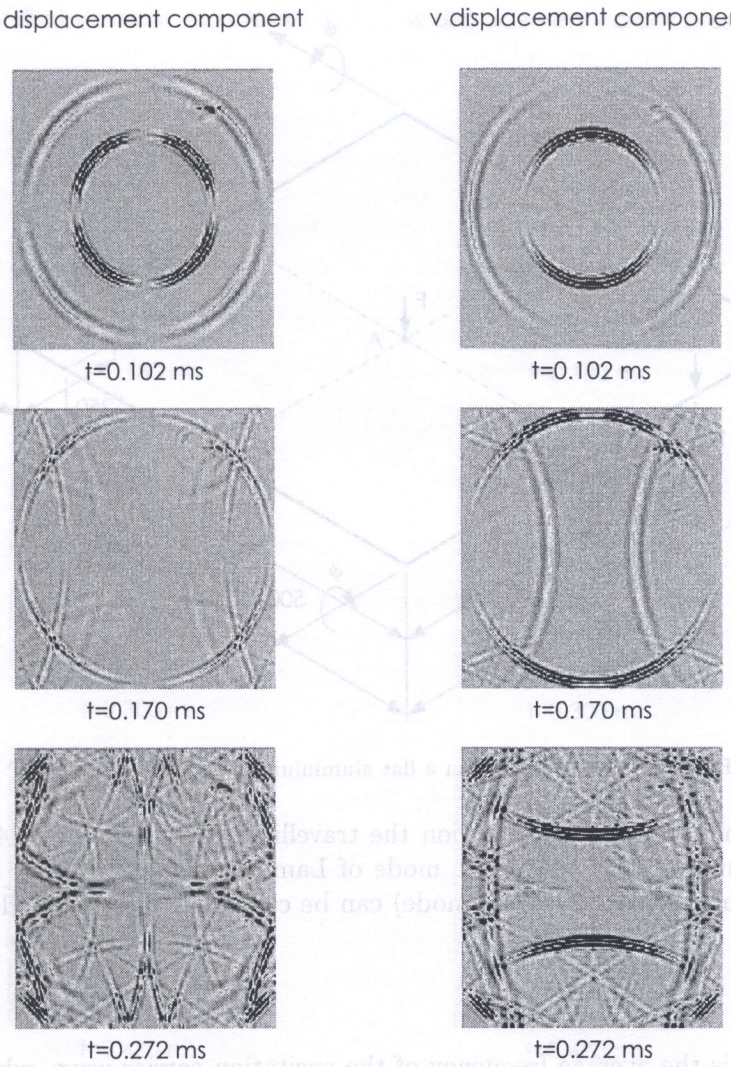

Fig. 12. Propagation of elastic waves in a flat aluminium panel with a crack

without the crack. As before, in this manner also the location of the crack can be evaluated, based on the known speeds c_p and c_s of the propagation of the elastic P and S waves in aluminium and by measuring the time lags between the reflected signals at the selected points.

3.4. Propagation of elastic waves in a flat isotropic plate

The geometry of a flat aluminium plate is presented in Fig. 13. In this analysis the plate has been divided into 1600 spectral plate finite elements of Reissner-Mindlin type, while each element has 36 nodes and 3 degrees of freedom per node (transverse displacement w and independent rotations ψ and ϕ). A force signal pulse F has been applied at the centre of the plate and in the direction of the z-axis.

The same as in the case of the previously discussed aluminium panel it has been assumed here that a transverse and open crack is located at the distance of 125 mm from top edge of the plate and 250 mm from the right edge. The assumed depth of the crack is 2 mm, which is equivalent to 20% of the plate thickness. Numerical calculation has been carried out for the plate with and without the crack and are presented as maps of displacements u and v at 3 different time instances in Figs. 11 and 12. The assumed type of boundary condition for the plate is the same as before and is of the free type (i.e. all for edges of the panel remain free).

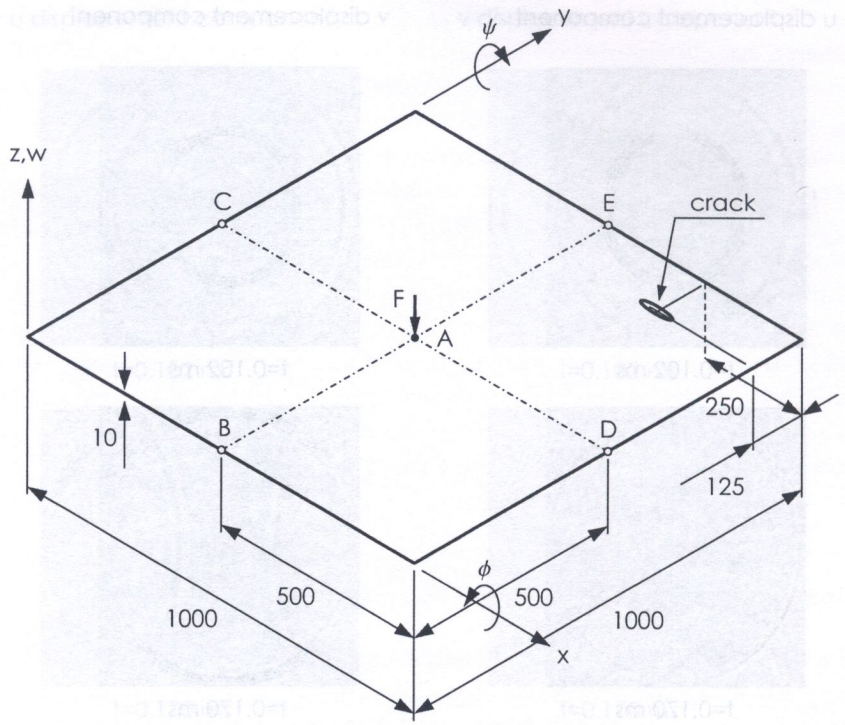

Fig. 13. The geometry on a flat aluminium plate with a crack

In the case of the plate under consideration the travelling waves are of the A type, exactly as in the case of the beam (i.e. anti-symmetric mode of Lamb waves). The speed c_0 of the wave in isotropic media (the phase speed of the A_0 mode) can be calculated from the following relation,

$$c_0 = \sqrt{\omega}\sqrt[4]{\frac{D}{\rho t}} \rightarrow c_0 = 3067.97 \text{ m/s}. \tag{14}$$

where $\omega = 2\pi f$ and f is the average frequency of the excitation carrier wave, which in the case of the excitation signal presented in Fig. 3 is equal to 100 kHz. The symbol D denotes the flexural stiffness of the plate and t is the plate thickness.

It should be pointed out that the same as in the case of the aluminium beam discussed before there are two modes A_0 and A_1 propagating in the plate at different propagation speeds. The presence of the higher mode A_1 is also due to the fact that the excitation signal has components of frequencies higher than the cut-off frequency f_c, for the given geometry and material of the plate. For excitation frequencies below the cut-off frequency f_c only the A_0 mode is propagating in the plate. On the other hand if the excitation frequency is higher than the cut-off frequency f_c, the higher A_1 mode is also observed. Obviously the presence of even higher modes A_2, A_3, etc., requires excitations above the appropriate cut-off frequencies.

The presence of the crack in the plate results in the wave propagation patter being more complex. Besides the waves reflected from the plate edges, and travelling as the modes A_0 and A_1, additional reflections from the crack location are also well visible, as shown in Fig. 14. The same as in the case of the beam discussed previously the reflections of either the mode A_0 or A_1 from the crack results in the generation of two new waves travelling as the modes A_0 and A_1.

As already mentioned, the amplitudes of these reflections are proportional to the size of the crack and they can be easily detected by measuring signals at a number of points located on the plate surface (for example at points A, B, C, D, and E as shown in Fig. 13) and by comparing them with the signals obtained in the case of the plate with no crack. In this way the location of the crack can be easily evaluated, based on the known speeds of the propagating A_0 and A_1 modes in aluminium and by measuring the time lags between the reflected signals at the selected points.

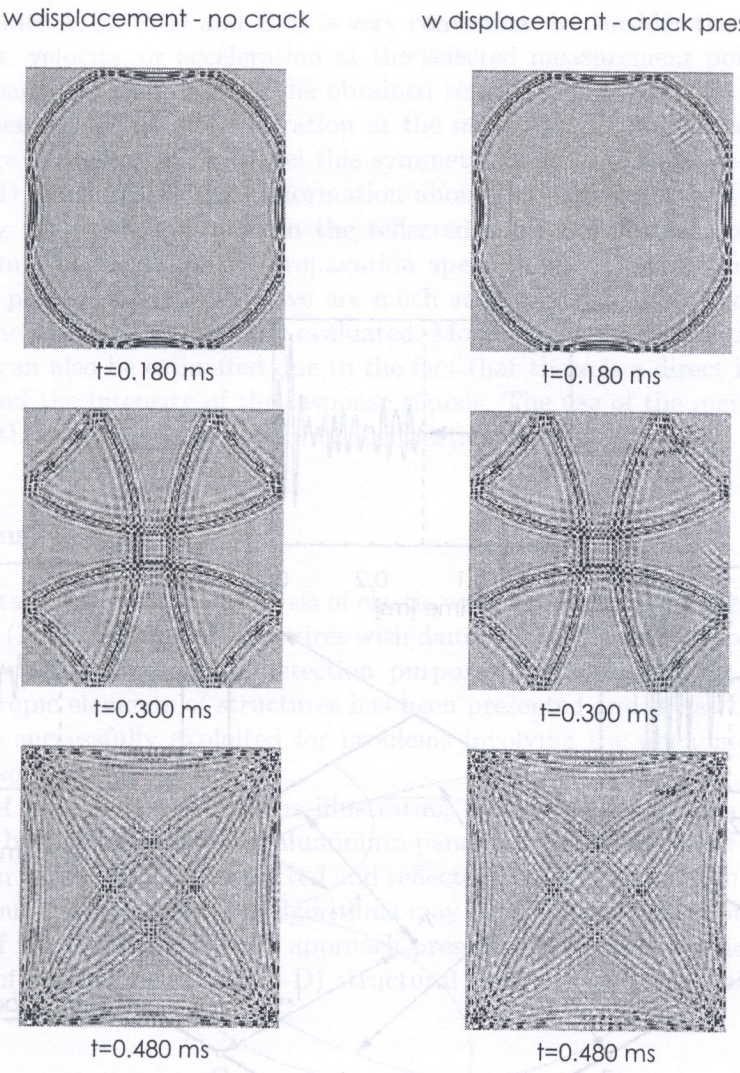

Fig. 14. Propagation of elastic waves in a flat aluminium plate with and without a crack

3.5. Damage detection concept

A simple concept for damage detection in isotropic elements of structures is presented in Fig. 15. However, the idea of this concept is explained on the case of the flat aluminium panel discussed previously, it can be straightforwardly applied or modified for the case of other elements of structures (curved or made out of anisotropic materials). This damage detection concept is based on differential response signals measured at a number of points located on the panel surface, which are the points A, B, C, D, and E.

The information about the presence of the damage in the panel becomes very clear when received response signals from the previously selected points are referred to certain *healthy* response signals acquired at the same points, and for the case of the panel with no damage. This can be achieved by considering the difference between the both response signals and producing so-called *differential* response signals in this way. Such differential response signals carry sufficient information in order to identify precisely not only the location of the damage, but also the extent of it.

It is worth pointing out that a right selection of the location of measurement points as well as displacement, velocity or acceleration components in order to obtain the differential response signal is a very important factor. Because the excitation signal is applied in the direction of the y-axis in the case of the investigated panel, and due the panel symmetry and the location of the

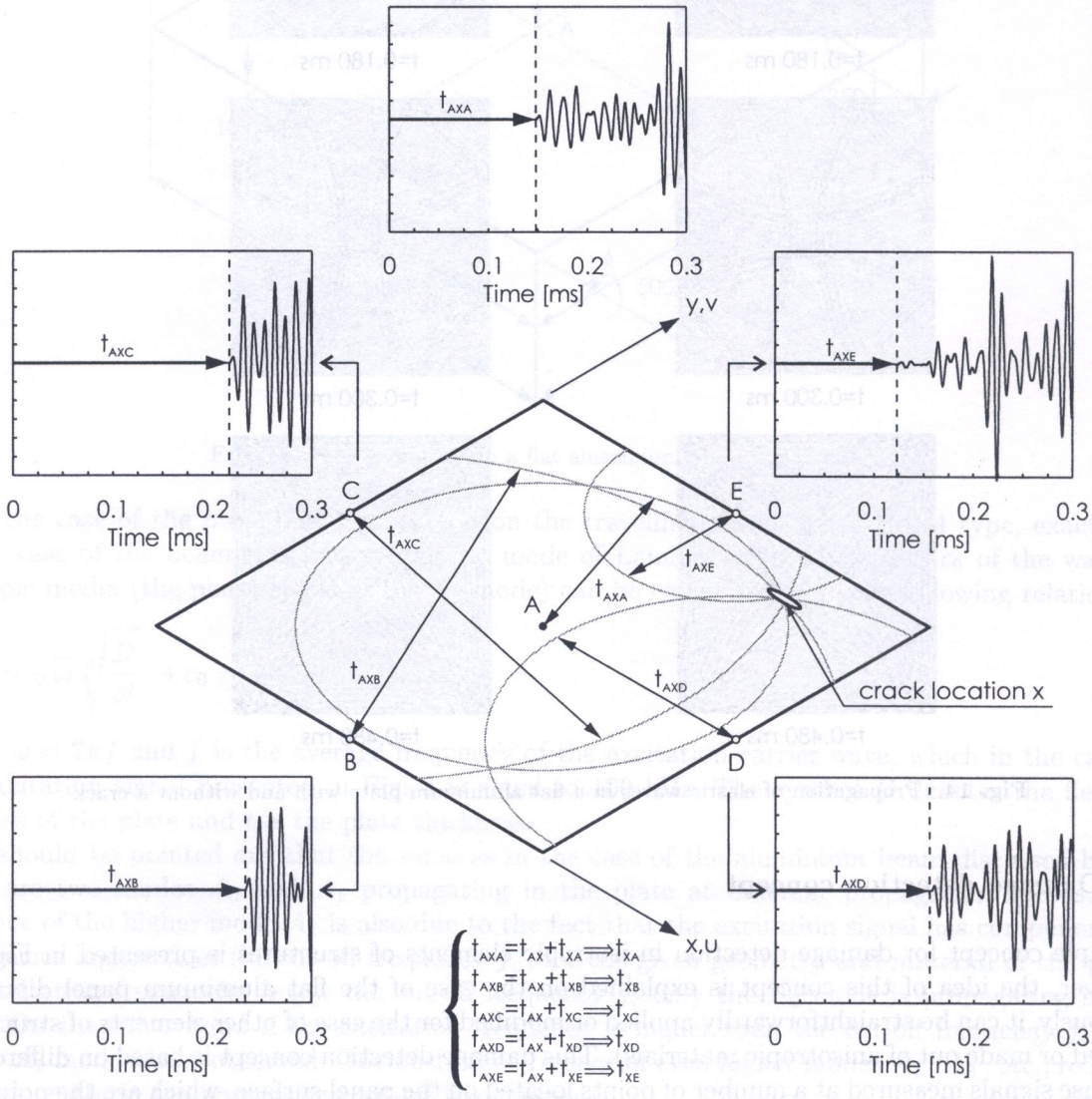

Fig. 15. Damage detection concept for the case of a flat isotropic panel

measurement points A, B, C, D and E, it is very convenient to consider the x components either of the displacement, velocity, or acceleration at the selected measurement points. This is because in the case of the panel with no damage the obtained response signal contain only the y components of the displacement, velocity, or acceleration at the measurement points (see Fig. 11). In the case when the damage is present in the panel this symmetry is distorted and the response signals from points A, B, C, D, and E carry then information about the damage.

By measuring the time lags between the reflected signals at the selected points, as shown in Fig. 15 and taking into account the propagation speed of the c_s wave (in the analysed case the response signals produced by the S wave are much stronger than those produced by the P wave) the location of the damage can be easily evaluated. Moreover, the extent of the damage (i.e. damage size and depth) can also be estimated due to the fact that there is a direct link between the extent of the damage and the intensity of the response signals. The use of the method of neural networks or genetic algorithms can be very helpful in this particular task.

3.6. Conclusions

In this paper certain results of the analysis of elastic wave propagation in one-dimensional (1-D) and two-dimensional (2-D) elements of structures with damage have been presented. Also the application of the obtained results for damage detection purposes has been shown. A concept for damage detection in isotropic elements of structures has been presented and it has been demonstrated that the SEM can be successfully exploited for problems involving the phenomena of the elastic wave propagation in isotropic media.

The results of numerical calculations illustrating the wave propagation in the case of an aluminium rod and beam as well as a flat aluminium panel and plate have been shown. The problem of damage detection based on the transmitted and reflected waves has been also considered. It has been shown that various damage detection algorithms may be developed based on the current approach. In the opinion of the authors the SEM approach presented can easily be modified and adopted for use in the case of three-dimensional (3-D) structural elements or structural elements made out of anisotropic or orthotropic materials.

Acknowledgments

The authors of this work would like to gratefully acknowledge the support for this research provided by the EU under the Sixth EU Framework Programme for Research and Technological Development (FP6) via ARTIMA project (Aircraft Reliability Through Intelligent Materials Application – reference number 502725), and also wish to thank the Polish Ministry of Scientific Research and Information Technology.

References

[1] C.A. Brebbia, J.C.F. Tells, L.C. Wrobel. *Boundary Elements Techniques*. Springer, Berlin, 1984.

[2] Y. Cho, J.L. Rose. A boundary element solution for mode conversion study of the edge reflection of Lamb waves. *Journal of the Acoustical Society of America*, **99**: 2079–2109, 1996.

[3] P.P. Delsanto, R.B. Mignogna. A spring model for the simulation of the ultrasonic pulses through imperfect contact interfaces. *Journal of Acoustical Society of America*, **104**: 1–8, 1998.

[4] P.P. Delsanto, T. Whitecomb, H.H. Chaskelis, R.B. Mignogna. Connection machine simulation of ultrasonic wave propagation in materials. I: the one-dimensional case. *Wave Motion*, **16**: 65–80, 1992.

[5] P.P. Delsanto, T. Whitecomb, H.H. Chaskelis, R.B. Mignogna, R.B. Kline. Connection machine simulation of ultrasonic wave propagation in materials. II: the two-dimensional case. *Wave Motion*, **20**: 295–314, 1994.

[6] P.P. Delsanto, R.S. Schechter, R.B. Mignogna. Connection machine simulation of ultrasonic wave propagation in materials. III: the three-dimensional case. *Wave Motion*, **26**: 329–339, 1997.

[7] J.F. Doyle. *Wave Propagation in Structures*. Springer-Verlag, New York, 1997.

[8] W. Dauksher, A.F. Emery. Accuracy in modeling the acoustic wave equation with Chebyshev spectral finite elements. *Finite Elements in Analysis and Design*, **26**: 115–128, 1997.

[9] B. Hackbush. *Multi-grid Methods and Applications*. Springer-Verlag, Berlin, 1985.

[10] I. Harari, E. Turkel. Accurate finite difference methods for time-harmonic wave propagation. *Journal of Computational Physics*, **119**: 252–270, 1995.

[11] H. Igawa, K. Komatsu, I. Yamaguchi, T. Kasai. Wave propagation analysis of frame structures using the spectral element method. *Journal of Sound and Vibration*, **277**: 1071–1081, 2004.

[12] M.H. Kim, W.C. Koo, S.Y. Hong. Wave interactions with 2D structures on/inside porous seabed by a two-domain boundary element method. *Applied Ocean Research*, **22**: 255–266, 2000.

[13] M. Kleiber. *Finite Element Method in Non-linear Continuum Mechanics (in Polish)*. PWN, Warsaw, 1985.

[14] D. Komatitsch, J.P. Violotte, R. Vai, J.M. Castillo-Covarrubias, F.J. Sanchez-Sesma. The spectral element method for elastic wave equation – Application to 2-D and 3-D seismic problems. *International Journal for Numerical Methods in Engineering*, **45**: 1139–1164, 1999.

[15] D. Komatitsch, C. Barnes, J. Tromp. Simulation of anisotropic wave propagation based upon a spectral element method. *Geophysics*, **4**: 1251–1260, 2000.

[16] D. Komatitsch, R. Martin, J. Tromp, M.A. Taylor, B.A. Wingate. Wave propagation in 2-D elastic media using a spectral element method with triangles and quadrangles. *Journal of Computational Acoustics*, **9**: 703–718, 2001.

[17] http://mathworld.wolfram.com/LegendrePolynomial.html.

[18] F. Moser, L.J. Jacobs, J. Qu. Modeling elastic wave propagation in waveguides with the finite element method. *NDT & E International*, **32**: 225–234, 1999.

[19] J. Orkisz. *Finite Difference Method (Part III), Handbook of Computational Solid Mechanics*. Springer-Verlag, Berlin, 336–432, 1998.

[20] A.T. Patera. A spectral element method for fluid dynamics: Laminar flow in a chanell expansion, *Journal of Computational Physics*, **54**: 468–488, 1984.

[21] M. Palacz, M. Krawczuk, W. Ostachowicz. The spectral finite element model for analysis of flexural-shear coupled wave propagation. Part 1: Laminated multilayer composite. *Composite Structures*, **68**: 37–44, 2005.

[22] S.Z. Peng. Flexural wave propagation and dynamic stress concentration in a multi-stepped plate using acoustical wave propagator method. *International Journal of Vehicle Noise and Vibration*, **1**: 169–182, 2004.

[23] E. Perrey-Debain, J. Trevelyan, P. Bettess. Plane wave interpolation in direct collocation boundary element method for radiation and wave scattering: numerical aspects and applications. *Journal of Sound and Vibration*, **261**: 839–858, 2003.

[24] C. Pozrikidis. *Introduction to Finite and Spectral Element Methods using MATLAB*, Taylor and Francis Group, LCC, San Diego, 2005.

[25] J.N. Reddy. *An Introduction to the Finite Element Method*. McGraw-Hill, Inc., Singapore, 1993.

[26] W.J. Staszewski. Ultrasonic/guided waves for structural health monitoring. *Key Engineering Materials, Trans. Tech. Publications*, **293-294**: 49–60, 2005.

[27] H. Yim, Y. Sohn. Numerical simulation and visualization of elastic waves using mass-spring lattice model. *IEEE Transactions on Ultrasonic, Ferroelectrics, and Frequency Control*, **47**: 549–558, 2000.

[28] X. Yu. Finite difference methods for the reduced water wave equation. *Computer Methods in Applied Mechanics and Engineering Volume*, **154**: 265–280, 1998.

[29] O.C. Zienkiewicz. *The Finite Element Method*. McGraw-Hill, London, 1989.

[30] F.I. Zyserman, P.M. Gauzellino. Dispersion analysis of a nonconforming finite element method for the three-dimensional scalar and elastic wave equations. *Finite Elements in Analysis and Design Volume*, **41**: 1309–1326, 2005.